# Intermolecular dissociation energies of hydrogen-bonded 1-naphthol complexes

Richard Knochenmuss, Rajeev K. Sinha, Anja Poblotzki, Takuya Den, and Samuel Leutwyler

Citation: J. Chem. Phys. **149**, 204311 (2018); doi: 10.1063/1.5055720
View online: https://doi.org/10.1063/1.5055720
View Table of Contents: http://aip.scitation.org/toc/jcp/149/20
Published by the American Institute of Physics

# Intermolecular dissociation energies of hydrogen-bonded 1-naphthol complexes

Richard Knochenmuss, Rajeev K. Sinha,[a] Anja Poblotzki,[b] Takuya Den, and Samuel Leutwyler[c]
*Department of Chemistry and Biochemistry, University of Bern, Freiestrasse 3, CH-3012 Bern, Switzerland*

(Received 10 September 2018; accepted 12 November 2018; published online 30 November 2018)

We have measured the intermolecular dissociation energies $D_0$ of supersonically cooled 1-naphthol (1NpOH) complexes with solvents S = furan, thiophene, 2,5-dimethylfuran, and tetrahydrofuran. The naphthol OH forms non-classical H-bonds with the aromatic $\pi$-electrons of furan, thiophene, and 2,5-dimethylfuran and a classical H-bond with the tetrahydrofuran O atom. Using the stimulated-emission pumping resonant two-photon ionization method, the ground-state $D_0(S_0)$ values were bracketed as 21.8 ± 0.3 kJ/mol for furan, 26.6 ± 0.6 kJ/mol for thiophene, 36.5 ± 2.3 kJ/mol for 2,5-dimethylfuran, and 37.6 ± 1.3 kJ/mol for tetrahydrofuran. The dispersion-corrected density functional theory methods B97-D3, B3LYP-D3 (using the def2-TZVPP basis set), and $\omega$B97X-D [using the 6-311++G(d,p) basis set] predict that the H-bonded (edge) isomers are more stable than the face isomers bound by dispersion; experimentally, we only observe edge isomers. We compare the calculated and experimental $D_0$ values and extend the comparison to the previously measured 1NpOH complexes with cyclopropane, benzene, water, alcohols, and cyclic ethers. The dissociation energies of the nonclassically H-bonded complexes increase roughly linearly with the average polarizability of the solvent, $\bar{\alpha}$(S). By contrast, the $D_0$ values of the classically H-bonded complexes are larger, increase more rapidly at low $\bar{\alpha}$(S), but saturate for large $\bar{\alpha}$(S). The calculated $D_0(S_0)$ values for the cyclopropane, benzene, furan, and tetrahydrofuran complexes agree with experiment to within 1 kJ/mol and those of thiophene and 2,5-dimethylfuran are ~3 kJ/mol smaller than experiment. The B3LYP-D3 calculated $D_0$ values exhibit the lowest mean absolute deviation (MAD) relative to experiment (MAD = 1.7 kJ/mol), and the B97-D3 and $\omega$B97X-D MADs are 2.2 and 2.6 kJ/mol, respectively. *Published by AIP Publishing.* https://doi.org/10.1063/1.5055720

## I. INTRODUCTION

Classical hydrogen bonds are considered to have important electrostatic and charge-transfer character, supplemented by smaller contributions from dispersion interactions.[1–5] The opposite holds for the weaker "nonclassical" OH···$\pi$, NH···$\pi$, CH··· O, or CH···$\pi$ hydrogen bonds.[3–6] The latter intermolecular interactions play important roles in the structure, stability, and the dynamic properties of peptides, proteins, open-chain nucleic acids, and tRNAs (transfer ribonucleic acids).[1–4,6]

Due to their comparative weakness, the accurate theoretical treatment of nonclassical hydrogen bonds is challenging. The introduction of dispersion-corrected density functionals tailored to include long-range correlation effects (DFT-D) has been a major advance.[7–12] However, the benchmark sets for intermolecular interactions on which the DFT-D dispersion corrections have been tested are themselves mostly based on calculations. Hobza and co-workers have created benchmark sets for noncovalent interactions of biochemical relevance, denoted S22,[13] S66,[14] S66a8,[15] and S66x8.[16] The calculated S22 interaction energies have later been improved by the groups of Szalewicz[17] and of Sherrill.[18] The recent NCIBLIND10 benchmark set for intermolecular interactions, which is based on 80 benchmark energies for 10 different dimers computed at the coupled-cluster with single, double and iterated triple excitations [CCSD(T)] level and using complete basis set extrapolations, is also entirely computational.[19] The non-covalent interaction energy part of the large GMTKN30 database[11,12] is also mainly based on calculations. Only six noble gas dimer dissociation energies[20,21] out of 95 noncovalent interaction energies in GMTKN30 are experimental values. The problems of theory ↔ theory benchmarking and advantages of experiment ↔ theory benchmarking were recently highlighted by Mata and Suhm.[22]

Thus, the ground-state intermolecular dissociation energies $D_0(S_0)$ of *nonclassically* H-bonded gas-phase complexes are important benchmark observables for testing theory. However, the number of experimental dissociation energies that can serve as benchmarks is still quite limited.[23–28] Neusser and co-workers have determined $D_0(S_0)$ values for the indole·benzene and 3-methylindole·benzene complexes, for which they postulated an NH···$\pi$ H-bond between the

[a]Permanent address: Department of Atomic and Molecular Physics, Manipal University, Manipal 576104, Karnataka, India
[b]Present address: Institut für Physikalische Chemie, Universität Göttingen, Tammannstrasse 6, 37077 Göttingen, Germany
[c]leutwyler@dcb.unibe.ch

indole and benzene moieties.[24,25,29] Knee *et al.* have inferred an excited-state dissociation energy $D_0(S_1) = 16.7 \pm 1.7$ kJ/mol for phenol·benzene using picosecond-resolved photofragment spectroscopy.[30] From this, one obtains a ground-state $D_0(S_0)$ of 15.0 ± 1.7 kJ/mol using the spectral shift of the electronic origin bands between phenol and phenol·benzene.[30,31] Zwier and co-workers determined the $D_0$ of the jet-cooled HOH···benzene complex to lie between 6.8 and 11.6 kJ/mol.[32] Courty *et al.* have subsequently narrowed this value to $D_0$ = 10.2 ± 0.4 kJ/mol.[33] Accurate dissociation energies of classically H-bonded dimers and small clusters containing $H_2O$, $D_2O$, and HCl have been measured by the Reisler group.[34–38]

The aim of this work is to provide new experimental $D_0(S_0)$ values of nonclassically and classically H-bonded gas-phase complexes as benchmarks for dispersion-corrected DFT methods and high-level correlated quantum chemical methods.[22,28,39–42] We have previously measured dissociation energies of complexes involving the 1-naphthol (1NpOH) UV chromophore using the stimulated emission pumping-resonant two-photon ionization (SEP-R2PI) method.[43–45] 1-Naphthol is small enough to be treated by high-level theoretical methods, but large enough to offer two intermolecular binding sites: Adsorption over the naphthalene ring gives rise to face structures that are dominantly bound by dispersion interactions,[43,46–52] whereas the OH group acts as an H-bond donor, giving rise to edge structures.[23,27,49,50,53] Recently, we have determined $D_0(S_0)$ values of 1NpOH face complexes with solvent atoms and molecules ranging from noble gases to *n*-alkanes,[49–52,54] where the adatom or admolecule interacts with the naphthalene rings via London dispersion interactions. However, the cyclopropane complex also forms an edge isomer that involves a non-classical H-bond from the OH group to a cyclopropane C-C bond.[49,51] 1NpOH also forms a non-classical OH···$\pi$ hydrogen bond with benzene, in which the $C_6$ axis of the benzene moiety lies roughly parallel to the 1-naphthol OH bond axis.[55] $D_0(S_0)$ values have also been measured for "classical" OH···O and OH···N hydrogen-bonded complexes of 1NpOH with the acceptors molecules $H_2O$, $D_2O$, methanol, ethanol, oxirane, oxetane, ammonia, and ammonia-$d_3$, which have localized lone-pair electrons on their heteroatoms.[27,53]

Below, we determine non-classical H-bond dissociation energies for the polar heteroaromatics furan and thiophene. We study the effect of aromaticity vs. non-aromaticity by comparing the furan and tetrahydrofuran (THF) complexes, where the latter forms a classical H-bond. We also measure the effect of adding methyl groups to furan by studying the 2,5-dimethylfuran (2,5-DMF) complex. Analogous methanol·furan and methanol·2,5-DMF complexes have been investigated by IR spectroscopy in slit supersonic jets, with a focus on the relative energies of the OH···O and OH···$\pi$ forms, also termed as an "intermolecular energy balance."[56–58] Here, we provide the absolute dissociation energy, albeit with 1-naphthol replacing methanol as an H-bond donor. Finally, we compare the experimental $D_0$ values to those calculated with the widely used dispersion-corrected density functional theory (DFT) methods B3LYP-D3, B97-D3, and $\omega$B97X-D.[8–11,59]

## II. METHODS

### A. The SEP-R2PI method

We have previously described the SEP-R2PI method,[28,49–51] which is schematically explained in Fig. S1 of the supplementary material. The supersonically cooled 1NpOH·S complexes are *pumped* by a ~5 ns pulsed tunable UV laser set to the electronic origin band of the $S_0 \rightarrow S_1$ transition, exciting the complex to the $S_1$; $v' = 0$ vibrationless level. A minor portion of the generated $S_1$ complexes is directly ionized by a second photon of the pump laser. In the following *dump* step, a second independently tunable UV laser transfers a large fraction of the $S_1$; $v' = 0$ population down to a specific $S_0$ state intra- or intermolecular vibrational level with $v_i'' > 0$. The dump laser is scanned toward low wavenumbers, corresponding to increasing $S_0$ state vibrational energy. Because of the large level density of the intra- and intermolecular vibrational modes even at low vibrational energy $E(v'')$, the microcanonically hot 1NpOH·S complexes undergo rapid intermolecular vibrational redistribution (IVR). The population transfer efficiency achieved in the SEP process [pump + dump + IVR] depends on the electronic oscillator strength $f_{el}$ and the Franck-Condon factors in absorption and (stimulated) emission and on the vibration-dependent IVR rates in the $S_0$ state. While other $S_1$ state processes such as internal conversion and intersystem crossing influence the overall SEP efficiency, they do not affect the SEP spectrum. After a 3 $\mu$s delay that allows IVR to go to completion, the microcanonically hot 1NpOH·S complexes are detected by R2PI with a third tunable UV pulsed laser, denoted the *probe* laser. This delay is long enough to permit the hot $S_0$ state complexes to couple to the intermolecular dissociative coordinates.[50,54]

For the $D_0(S_0)$ measurement, we first determine the energies of the optically active $S_0(v_i'' > 0)$ vibrational levels by recording the *decrease* of the R2PI ion signal of the 1-naphthol·S complex in the pump + dump step while scanning the dump laser. Alternatively, the dispersed fluorescence emission spectrum is excited at the $0_0^0$ band; see Fig. S1. Both the dump and fluorescence spectra are $S_1$; $v' = 0 \rightarrow S_0$ vibronic spectra, which have identical $f_{el}$ and Franck-Condon factors. However, the band intensities may differ because the dump spectra depend on the $S_0$ state IVR, which depletes the lower state, while the fluorescence spectrum does not. Below we will show the spectrum that exhibits the better signal/noise ratio. In the second measurement, the probe laser is fixed at a hot band (or sequence band) of the 1NpOH·S complex that originates from a $v'' > 0$ level, so the dump transitions are detected as positive-going *hot-band* SEP-R2PI signals. Hot-band SEP signals are only observed if the microcanonically hot $S_0$ state 1NpOH·S complex remains bound during the entire 3 $\mu$s pump-probe delay time; see Fig. S1 of the supplementary material. If the dump laser excites vibrations of 1NpOH·S that lie above $D_0(S_0)$ and IVR is followed by 1NpOH ↔ S vibrational predissociation, the complex falls apart during the 3 $\mu$s delay and the hot-band SEP-R2PI spectrum breaks off. The ground-state dissociation energy $D_0(S_0)$ of the complex is bracketed between the highest-wavenumber dump transition observed in the hot-band SEP spectrum and the lowest-wavenumber band that

is *not* observed in the hot-band SEP spectrum, but appears in the dump or dispersed fluorescence spectra.

### B. Experimental

The supersonically cooled 1NpOH·S complexes were produced by co-expanding 1NpOH (Fluka, 99%) and 0.1%-0.2% of furan, thiophene, 2,5-DMF, or THF (Sigma-Aldrich, purity >99%). The admolecules were premixed in a Ne carrier gas, and the total backing pressures were 1.4-1.6 bars. The 1NpOH was heated to 347 K (0.3 mbar vapor pressure). Two frequency-doubled tunable dye lasers (Lambda Physik FL2002 and FL3002, fundamental range 620-660 nm) were employed as pump (0.5-1 mJ/pulse) and dump (1-2 mJ/pulse) lasers, both pumped by the same Nd:YAG laser (Innolas Spitlight 600). The probe dye laser (Lambda Physik LPD 3000, ~0.3 mJ/pulse) was pumped by a Continuum Surelite II frequency-doubled Nd:YAG laser. The dye-laser wavelength and bandwidths before frequency doubling were monitored using a HighFinesse WS6 wavemeter; the bandwidths were 0.3-0.4 $cm^{-1}$. The probe laser was time-delayed by 3 $\mu$s and crossed the molecular beam 3 mm downstream of the pump and dump lasers to compensate for the ~950 m/s mean speed of the molecular beam. Other experimental details are as reported previously.[49–52]

Mass-selective one-color resonant two-photon ionization (R2PI) spectra[49–52] were recorded by exciting and ionizing the 1NpOH·S complexes in the ion-source of a 120 cm long linear time-of-flight mass spectrometer. UV/UV hole-burning spectra were also measured for all complexes. $S_1 \rightarrow S_0$ dispersed fluorescence spectra were measured by exciting the $0_0^0$ band of the respective complex isomer. The fluorescence emission was collected with fused silica optics and detected in the second order of a SOPRA UHRS F1500 1.5 m monochromator using a Hamamatsu R928 photomultiplier. The slit width was 200 $\mu$m, equivalent to a bandpass of 28 pm (~3 $cm^{-1}$), and the spectra were scanned in 2.5 pm steps.

### C. Theoretical methods

The minimum-energy structures and harmonic vibrational frequencies of the 1NpOH·S complexes were calculated with three different dispersion-corrected density functional theory (DFT-D) methods. The B97-D3[7] and B3LYP-D3[60] methods were employed with the def2-TZVPP basis set using Gaussian16.[61] For comparison, we employed the Chai-Gordon long-range and dispersion-corrected $\omega$B97X-D functional,[9] as implemented in Gaussian16,[61] using the 6-31++G(d,p) basis set. The latter two methods have given good results in studies of large $\pi$-stacked complexes.[62,63] All structure optimizations were unconstrained. The binding energies $D_e$ were calculated by subtracting the total energies of *trans*-1-naphthol and of the solvent molecule S—both optimized at their respective isolated-molecule geometries—from the total energy of the 1-naphthol·S complex at its optimized minimum-energy geometry. The Boys-Bernardi counterpoise (CP) correction for basis set superposition error (BSSE) was used for the $\omega$B97X-D calculation. With the def2-TZVPP basis set, the BSSE effects start to be negligible,[7] and we did not perform CP corrections. The larger def2-QZVPP basis set led to prohibitively large computational costs and could not be employed.

The harmonic frequencies and vibrational zero point energies (VZPEs) of the monomers and complexes were calculated with all three DFT methods at the same level as the optimized structures. The dissociation energies $D_0$ were calculated as $D_0 = D_e - \Delta$VZPE using the *change* in zero-point energies $\Delta$VZPE, given by $\Delta$VZPE = VZPE(complex) − VZPE(1NpOH) − VZPE(*n*-alkane). For all complexes investigated here, the DFT-D calculations predict both face and edge structures. The latter are predicted to be more strongly bound than the face isomers, which is confirmed by the experiment.

## III. RESULTS

### A. Resonant two-photon ionization spectra

Figure 1 shows the one-color R2PI spectra of bare 1-naphthol and of the 1-naphthol·S complexes with S = thiophene, furan, 2,5-DMF, and THF in the region of their $S_0 \rightarrow S_1$ $0_0^0$ bands. The spectra in Figs. 1(b)–1(e) exhibit weak vibronic bands that correspond to the excitation of $S_1$ state intermolecular vibrational fundamentals and overtones or combinations thereof. These give information on the intermolecular frequencies. In Fig. 1, we also indicate band assignments of different isomers (A, B, and C) of the furan and THF

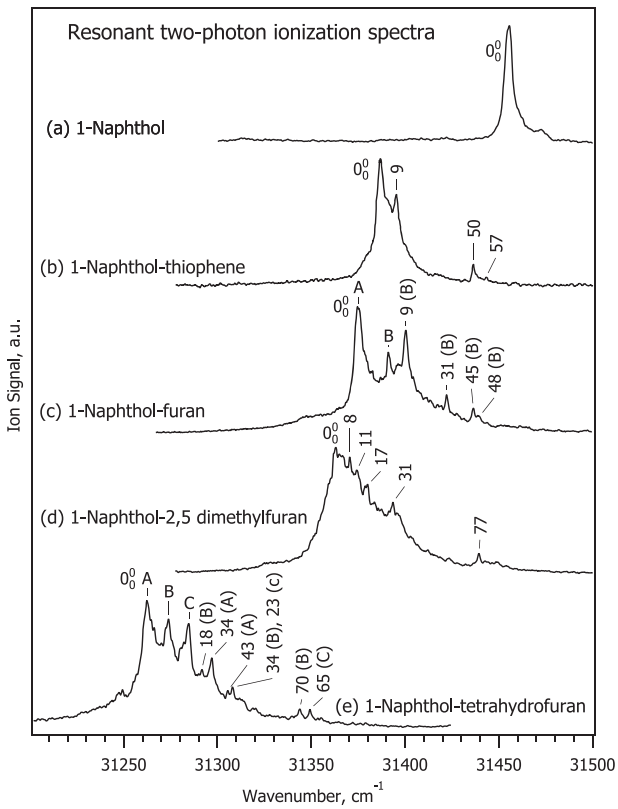


FIG. 1. One-color resonant-two-photon ionization spectra of (a) 1-naphthol and its complexes with (b) thiophene, (c) furan, (d) 2,5-dimethylfuran, and (e) tetrahydrofuran. The R2PI and UV-holeburned spectra of the furan and tetrahydrofuran complexes are shown in Figs. S2 and S3 of the supplementary material. The most intense $S_1$ state intermolecular vibronic bands are labeled with their relative wavenumber; for assignments, see Table I.

complexes, which were established by UV/UV hole-burning spectroscopy; see below.

The $0_0^0$ bands of the complexes are shifted relative to the 1-naphthol $0_0^0$ (at 31 455.7 $cm^{-1}$) by the spectral shift $\delta\tilde{\nu}$. A thermochemical cycle[47,64,65] shows that $\delta\tilde{\nu}$ corresponds to the *difference* of the ground- and excited-state dissociation energies, $\delta\tilde{\nu} = D_0(S_0) - D_0(S_1)$; see also Fig. S1. The spectral shift is empirically observed to be a good predictor of the binding topology of 1NpOH·S complexes.[49–52,54] The face complexes exhibit small spectral shifts between $\delta\tilde{\nu} = +5$ and $-10$ $cm^{-1}$; e.g., the face isomer of 1NpOH·cyclopropane exhibits a small blue shift of $\delta\tilde{\nu} = +2$ $cm^{-1}$. The spectral shifts of the edge complexes are large and to the red, and thus $\delta\tilde{\nu} = -72$ $cm^{-1}$ for the edge isomer of 1NpOH·cyclopropane.[49]

### 1. 1-Naphthol·thiophene

The R2PI spectrum in Fig. 1(b) shows an intense $S_0 \rightarrow S_1$ electronic origin at 31 387 $cm^{-1}$, which is red-shifted by $\delta\tilde{\nu} = -69$ $cm^{-1}$, indicating that this is an edge complex. UV/UV holeburning measurements revealed that the entire spectrum arises from a single isomer. We assign the bands at $0_0^0 + 9$, +50, and +57 $cm^{-1}$ as fundamentals of the intermolecular vibrations $\nu'_X$ (calculated at 14 $cm^{-1}$) and $\nu'_{rot,1}$ (calculated at 55 $cm^{-1}$) and a weak combination band $\nu'_X + \nu'_{rot,1}$. The calculated intermolecular B97-D3 frequencies are given in Table I.

### 2. 1-Naphthol·furan

UV/UV spectral holeburning of 1NpOH·furan reveals that two isomers contribute to the R2PI spectrum in Fig. 1(c). The isomer spectra are shown in Fig. S2 of the supplementary material. They overlap strongly, and isomer separation by UV/UV-holeburning was only partially possible. The more strongly populated isomer, which we denote as A, exhibits a strong origin band that is redshifted by $\delta\tilde{\nu} = -81$ $cm^{-1}$. Isomer B contributes about 30% to the spectrum, and its spectral shift is slightly smaller than that of isomer A, making the separation of the contributions difficult. Its intermolecular vibrational bands, four of which are marked by (B) in Fig. 1(c), also overlap with those of isomer A. For this reason, the $0_0^0$ band of isomer B could not be definitely located and the dissociation energies of the furan complex could not be measured separately for the two isomers. Since the spectral shifts are large, we assign both isomers as hydrogen-bonded edge structures.

### 3. 1-Naphthol·2,5-dimethylfuran

The one-color R2PI spectrum of the 1NpOH·2,5-DMF complex in Fig. 1(d) is spectrally shifted by $\delta\tilde{\nu} = -93$ $cm^{-1}$, slightly farther than the furan complex. We also assign it as an edge complex. UV/UV spectral holeburning shows that the entire spectrum arises from a single isomer. The $0_0^0$ band is considerably broader than those of the thiophene and furan complexes, and we interpret this as arising from a stronger coupling of the $S_0 \rightarrow S_1$ electronic excitation to the low-frequency intermolecular vibrations. This implies that the intermolecular coordinates of the DMF complex undergo a larger change upon electronic excitation than the other complexes. We assign the bands observed at 8, 11, 31, and 77 $cm^{-1}$ above the $0_0^0$ band to the fundamentals of the intermolecular vibrations $\nu'_X$ (calculated to be 4.5 $cm^{-1}$), $\nu'_Y$ (calculated 20 $cm^{-1}$), $\nu'_Z$ (calculated 47 $cm^{-1}$), and $\nu'_{rot,3}$ (calculated 77 $cm^{-1}$). The calculated intermolecular B97-D3 frequencies are also included in Table I.

### 4. 1-Naphthol·tetrahydrofuran

The R2PI spectrum in Fig. 1(e) shows an intense and well-structured electronic origin at 31 262 $cm^{-1}$. The spectral shift is $\delta\tilde{\nu} = -194$ $cm^{-1}$, about twice that of the 2,5-DMF complex and more than twice that of the furan complex. The spectral shift is close to that of the 1NpOH·oxetane complex ($\delta\tilde{\nu} = -184$ $cm^{-1}$).[27] Oxetane and THF are homologous four- and five-ring cyclic ethers, so the similarity of the spectral shifts also implies an edge structure. UV/UV holeburning spectra revealed that at least three isomers contribute to the $0_0^0$ band in Fig. 1(e). We denote these as A, B, and C, and their respective spectral shifts are $\delta\tilde{\nu} = -194, -183$, and $-172$ $cm^{-1}$. As for the furan complex, it was difficult to separate the R2PI spectra by UV/UV holeburning due to the overlap of the three isomers.

The free THF molecule undergoes pseudorotational isomerization across low potential energy barriers, leading to two equivalent "envelope," two equivalent "twisted," and four equivalent asymmetric stationary points on the THF potential-energy surface.[66] These pseudorotational conformations may freeze into different minima upon jet-cooling and complex

TABLE I. Experimental and B97-D3 calculated intermolecular fundamental frequencies and changes of vibrational zero-point energies ΔVZPEs (in $cm^{-1}$) of the 1-naphthol·S hydrogen-bonded complexes with S = furan, thiophene, 2,5-dimethylfuran, and tetrahydrofuran.

| | Experimental frequencies | | | | | | B97-D3 harmonic frequencies | | | | | | ΔVZPE (B97-D3 calc.) | | |
|---|---|---|---|---|---|---|---|---|---|---|---|---|---|---|---|
| Admolecule S | $\tilde{\nu}_X$ | $\tilde{\nu}_Y$ | $\tilde{\nu}_Z$ | $\tilde{\nu}_{rot,1}$ | $\tilde{\nu}_{rot,2}$ | $\tilde{\nu}_{rot,3}$ | $\tilde{\nu}_X$ | $\tilde{\nu}_Y$ | $\tilde{\nu}_Z$ | $\tilde{\nu}_{rot,1}$ | $\tilde{\nu}_{rot,2}$ | $\tilde{\nu}_{rot,3}$ | inter | Δ intra | Total |
| Furan[a] | 9 | 31 | 45 | ··· | ··· | ··· | 3.9 | 30.6 | 38.8 | 57.9 | 71.0 | 81.6 | 142(53%) | 128(47%) | 270 |
| Thiophene[b] | 9 | ··· | ··· | 50 | ··· | ··· | 14.2 | 21.8 | 37.2 | 59.1 | 68.6 | 90.0 | 145(62%) | 89(38.0%) | 235 |
| 2,5-Dimethylfuran[c] | 8 | 11 | 31 | ··· | ··· | 77 | 4.5 | 20.3 | 46.6 | 55.0 | 72.9 | 77.3 | 138(38%) | 223(62%) | 361 |
| Tetrahydrofuran[d] | ··· | 34 | 43 | ··· | ··· | ··· | 29.1 | 60.6 | 78.0 | 13.8 | 99.8 | 117.9 | 200(39%) | 309(61%) | 509 |

[a]Calculated values are for isomer 1.
[b]Calculated values are for isomer 2.
[c]Calculated values are for isomer 1.
[d]Calculated values are for isomer 1.

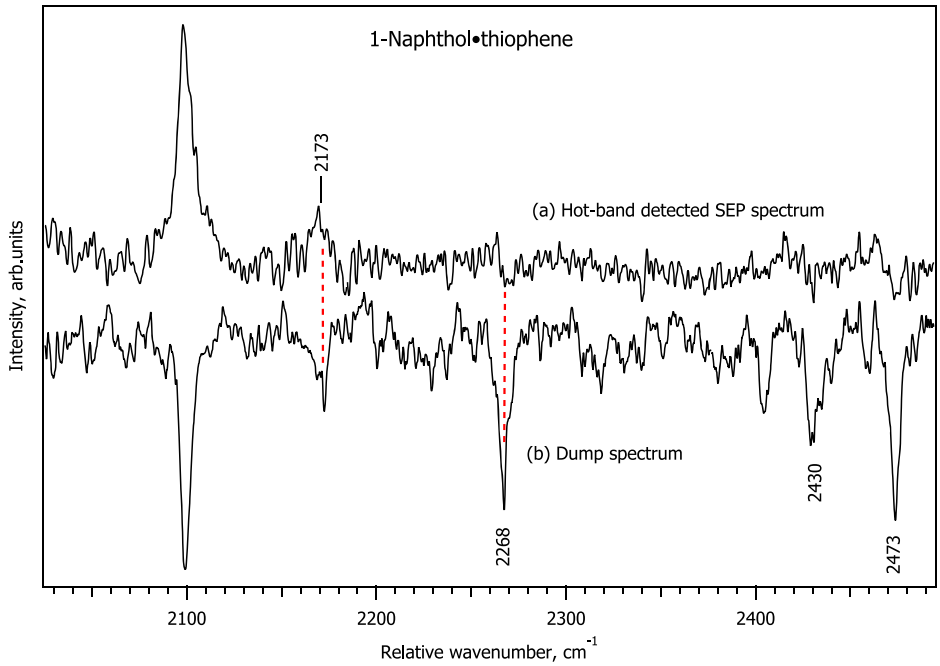


FIG. 2. (a) Hot-band probed SEP-R2PI and (b) dump spectra of the 1-naphthol·thiophene complex. The x-axis is the difference between the pump and dump laser wavenumber. The $D_0(S_0)$ is bracketed by the highest-energy vibronic level at 2173 $cm^{-1}$ observed in spectrum (a) and the next higher band at 2268 $cm^{-1}$ that appears in the dump spectrum (b), but not in (a); see the vertical red dashed lines.

formation. This would explain the formation of isomers with only slightly different spectral shifts. Increasing the stagnation pressure decreases the vibrational temperature of the complex and changes the shape of the $0_0^0$ band: The contributions from isomers A and C decrease strongly relative to that of isomer B, but they still contribute to the width of the band. At lower temperatures, the lowest-energy band shifts slightly to the blue, to 31 273 $cm^{-1}$. The corresponding R2PI spectra are shown in Fig. S3 of the supplementary material. As for the furan complex, the dissociation energies $D_0$ of the THF complex isomers could not be measured separately.

## B. Experimental dissociation energies

### 1. 1-Naphthol·thiophene

Figure 2(a) shows the hot-band probed SEP-R2PI spectrum, which was measured with the probe laser set to a broad hot-band signal at $0_0^0 - 47$ $cm^{-1}$, as shown in Fig. S4 of the supplementary material. The R2PI spectrum of pump/dumped 1NpOH·thiophene is also shown in Fig. S4. The dump spectrum of 1NpOH·thiophene in Fig. 2(b) is similar to the hot-band SEP spectrum in Fig. 2(a) up to the band at 2173 $cm^{-1}$. The following vibronic band at 2268 $cm^{-1}$ and subsequent bands to higher energy in Fig. 2(b) are not observed in (a). Thus, the 2173 $cm^{-1}$ and the 2268 $cm^{-1}$ bands in Fig. 2 bracket the ground-state $D_0(S_0)$ of the 1NpOH·thiophene complex as $2221 \pm 48$ $cm^{-1}$. The excited-state dissociation energy $D_0(S_1)$ is obtained by subtracting the experimental spectral shift of the origin band ($\delta\tilde{\nu} = -69$ $cm^{-1}$) from the $D_0$ of the ground state, giving $D_0(S_1) = 2290 \pm 48$ $cm^{-1}$; see also Table II.

Note that the ± limits mentioned below are the limits of the bracketing interval and should *not* be taken as the statistical standard deviation of the experimental mean value of the measurement. The true dissociation energy may lie *anywhere* within the bracketed interval with equal probability.

### 2. 1-Naphthol·furan

Figure 3(a) shows the hot-band probed SEP-R2PI spectrum of 1NpOH·furan with the probe laser set to $0_0^0 - 83$ $cm^{-1}$.

TABLE II. Experimental dissociation energies $D_0(S_0)$ and $D_0(S_1)$ and spectral shifts $\delta\tilde{\nu}$ of hydrogen bonded 1-naphthol·S complexes. The true $D_0$ may lie anywhere within the bracketed interval with equal probability.

| | $D_0(S_0)$ | | $D_0(S_1)$ | | $\delta\tilde{\nu}$ |
|---|---|---|---|---|---|
| Adduct | $cm^{-1}$ | kJ/mol | $cm^{-1}$ | kJ/mol | $cm^{-1}$ |
| Thiophene | 2221 ± 48 | 26.56 ± 0.57 | 2290 ± 48 | 27.38 ± 0.47 | −69 ± 1 |
| Furan | 1824 ± 24 | 21.82 ± 0.29 | 1905 ± 25 | 22.79 ± 0.29 | −81 ± 1 |
| 2,5-Dimethylfuran | 3052 ± 191 | 36.5 ± 2.3 | 3145 ± 191 | 37.6 ± 2.3 | −93 ± 1 |
| Tetrahydrofuran | 3146 ± 108 | 37.63 ± 1.29 | 3328 ± 108 | 39.66 ± 1.29 | −182 ± 1 |
| Cyclopropane edge[a] | 1283 ± 3 | 15.34 ± 0.03 | 1354 ± 3 | 16.20 ± 0.04 | −72 ± 1 |
| Benzene[b] | 1773 ± 25 | 21.21 ± 0.30 | 1839.5 ± 25 | 22.00 ± 0.30 | −66 ± 1 |
| Benzene-$d_6$[b] | 1778 ± 21 | 21.26 ± 0.25 | 1884 ± 21 | 22.53 ± 0.25 | −66 ± 1 |

[a]From Ref. 49.
[b]From Ref. 23.

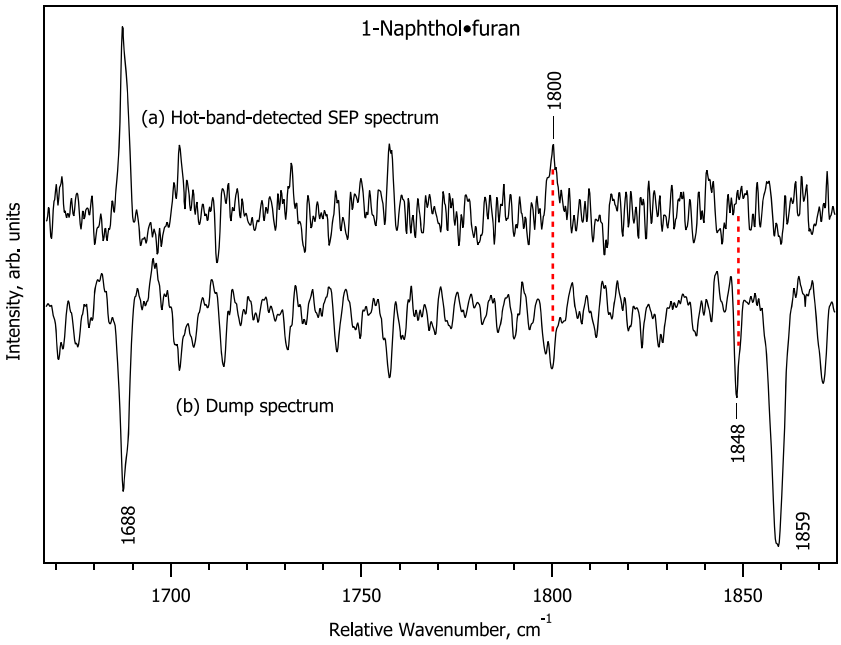


FIG. 3. (a) Hot-band probed SEP-R2PI and (b) dump spectra of the 1-naphthol·furan complex. The x-axis is the difference between the pump and dump laser wavenumber. The $D_0(S_0)$ is bracketed by the highest-energy vibronic level at 1800 $cm^{-1}$ observed in spectrum (a) and the next higher band at 1848 $cm^{-1}$ that appears in spectrum (b) but not in (a); see the vertical red dashed lines.

The pump laser was set to the $0_0^0$ band of isomer A at 31 375 $cm^{-1}$; see Fig. 1(c). As discussed in Sec. III A, this band overlaps with the $0_0^0$ band of isomer B, so the SEP-R2PI measurement does not discriminate between the two isomers.

The dump spectrum in Fig. 3(b) mirrors the hot-band SEP spectrum in Fig. 3(a) up to 1800 $cm^{-1}$. The following bands at 1848 $cm^{-1}$ and above in the dump spectrum in Fig. 3(b) are not observed in spectrum (a). Note that the 1800 $cm^{-1}$ band corresponds to the lower $D_0$ limit of the *more stable* ground-state isomer (the signal breakoff from the minor isomer B might go unnoticed if its $D_0$ were smaller). Thus, the 1800 and 1848 $cm^{-1}$ bands in Figs. 3(a) and 3(b) bracket the $D_0(S_0)$ of the more stable isomer of 1NpOH·furan as 1824 ± 24 $cm^{-1}$. The excited-state dissociation energy $D_0(S_1)$ = 1905 ± 25 $cm^{-1}$ is obtained from the spectral shift of the $0_0^0$ band ($\delta\tilde{\nu} = -81$ $cm^{-1}$); see also Table II.

### 3. 1-Naphthol·2,5-dimethylfuran

Figure 4(a) shows the hot-band probed SEP-R2PI spectra of 1NpOH·2,5-DMF. The pump laser was set to the $0_0^0$ band and the probe laser to $0_0^0$ − 34 $cm^{-1}$. The fluorescence

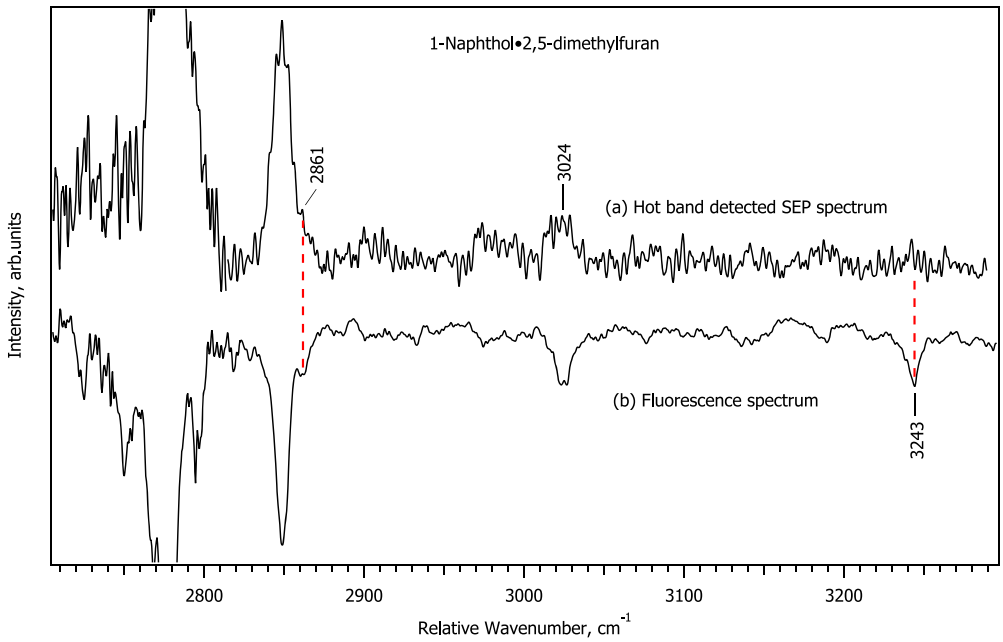


FIG. 4. (a) Hot-band probed SEP-R2PI and (b) fluorescence spectra of the 1-naphthol·2,5-dimethylfuran complex. The fluorescence spectrum was excited at the $0_0^0$ band (31 362 $cm^{-1}$). For (a), the x-axis is the difference between the pump and dump laser wavenumber and for (b) the difference between the pump and fluorescence wavenumber. The $D_0(S_0)$ is bracketed by the highest-energy vibronic level at 2861 $cm^{-1}$ observed in spectrum (a) and the next higher band at 3243 $cm^{-1}$ in the fluorescence spectrum; see the vertical red dashed lines.

spectrum of this complex shown in Fig. 4(b) exhibits better signal/noise ratio than the dump spectrum. Mirror symmetry between the two spectra is observed up to and including a weak band at 3024 $cm^{-1}$. The next significant band in the fluorescence spectrum is observed at 3243 $cm^{-1}$, but this and the following vibronic bands in the fluorescence spectrum are not observed in spectrum Fig. 4(a). Thus, at first sight, the 3024 and 3243 $cm^{-1}$ bands in Fig. 4 bracket the $D_0(S_0)$ of 1NpOH·2,5-DMF as 3134 ± 110 $cm^{-1}$.

However, this experimental $D_0$ is 15%-25% larger than the three DFT-D calculated values discussed below. By contrast, the calculated $D_0$ values for 1NpOH·furan and 1NpOH·THF lie close to or within the experimental $D_0$ brackets. The good agreement between experiment and theory for the furan and THF complexes but not for the 2,5-DMF complex calls for a closer examination. In previous work on the SEP-R2PI detected dissociation energies of 1NpOH·methane and 1NpOH·ethane, we noted weak bands in the hot-band detected SEP spectra that we interpreted as long-lived metastable vibrational levels lying above the putative dissociation limit.[54] The metastability was tentatively explained in terms of the large contribution of the low-wavenumber methane or ethane surface-rotational and internal-rotation modes to the vibrational level density $\rho_{vib}$, combined with the weak coupling of these IVR-populated states to the intermolecular dissociation coordinate.[54] For the methane and ethane complexes, the $D_0$ brackets were revised downward accordingly.[54]

Given the two methyl groups of 2,5-DMF, the weak vibronic band at 3024 $cm^{-1}$ might correspond to a level that is metastable with respect to vibrational predissociation. The two lowest calculated vibrations of 2,5-DMF are indeed methyl torsions, but with calculated harmonic wavenumbers of 132 and 145 $cm^{-1}$, these are 2-30 times larger than the harmonic frequencies of the six intermolecular modes given in Table I. Thus, while the two methyl torsions of 2,5-DMF do contribute to the $\rho_{vib}$ of the complex, they do not dominate it to the extent that occurs in the methane and ethane complexes. The intermolecular and methyl-rotor vibrations are highly anharmonic, so it is not currently possible to accurately calculate the anharmonic $\rho_{vib}$ required to discuss these effects quantitatively. Also, there might be nuclear-spin symmetry restrictions on the methyl-rotor states that affect both the IVR into and the vibrational predissociation of these levels. We conclude that the 3024 $cm^{-1}$ level is a borderline case: If it is indeed metastable, it is an upper limit to $D_0$, the lower limit then being determined by the band at 2861 $cm^{-1}$. We therefore give conservatively estimated brackets 2861 and 3243 $cm^{-1}$, as indicated in Fig. 4, leading to $D_0(S_0)$ = 3052 ± 191 $cm^{-1}$. With the spectral shift $\delta\tilde{\nu}$ = −93 $cm^{-1}$ of the $0_0^0$ band, we obtain the excited-state dissociation energy $D_0(S_1)$ = 3145 ± 191 $cm^{-1}$; see also Table II.

### 4. 1-Naphthol·tetrahydrofuran

Figure 5(a) shows the hot-band probed SEP-R2PI spectrum of the 1NpOH·THF complex, with the pump laser set to the $0_0^0$ band of isomer B, The probe laser was set to $0_0^0$ − 63 $cm^{-1}$; see Fig. S5 of the supplementary material. Note that isomers A and C are also optically excited at this wavenumber, albeit less strongly. Similar to the 1-naphthol·furan measurement, this $D_0$ determination is not isomer-selective. The fluorescence spectrum upon excitation at 31 274 $cm^{-1}$ is shown in Fig. 5(b). In trace (a), the spectrum breaks off at the weak vibronic band at 3038 $cm^{-1}$. The lowest-energy vibronic band that is *not* observed in Fig. 5(a) lies at 3253 $cm^{-1}$. Thus, the two bands at 3038 and 3253 $cm^{-1}$ in Fig. 5 bracket the $D_0(S_0)$ of 1NpOH·THF complex as

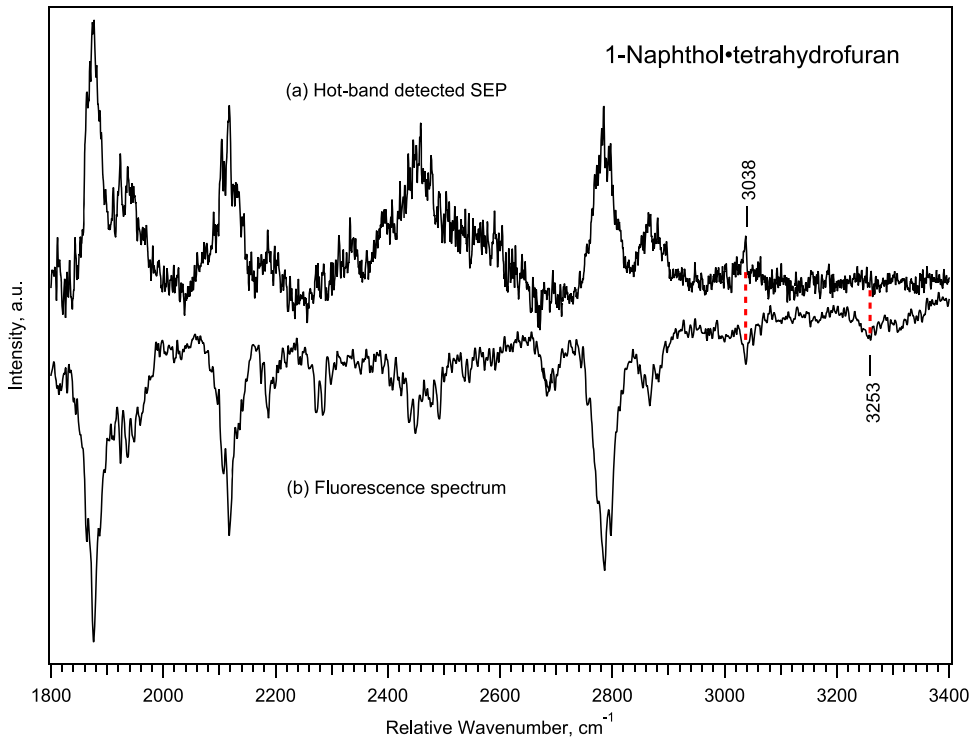


FIG. 5. (a) Hot-band detected SEP-R2PI and (b) fluorescence spectra of the 1-naphthol·tetrahydrofuran complex. The fluorescence spectrum was excited at the $0_0^0$ band of isomer B (31 274 $cm^{-1}$); see Fig. 1(e). The x-axis is defined as in Fig. 4. The $D_0(S_0)$ is bracketed by the highest-energy vibronic band at 3038 $cm^{-1}$ in spectrum (a) and the next higher band at 3253 $cm^{-1}$ in the fluorescence spectrum indicated by the vertical red dashed lines.

3146 ± 108 $cm^{-1}$; see Table II. With the spectral shift $\delta\tilde{\nu}$ = −182 $cm^{-1}$, we obtain the excited-state dissociation energy $D_0(S_1)$ = 3328 ± 108 $cm^{-1}$; see also Table II.

### C. Calculated structures

The B97-D3, B3LYP-D3, and ωB97X-D calculated lowest energy structures are always edge isomers. We located and optimized two edge isomers of the thiophene and 2,5-DMF complexes, three isomers of the furan complex, and four isomers of the THF complex. We also optimized a face isomer for the thiophene, furan, and 2,5-DMF complexes. However, these are local minima that lie 7-12 kJ/mol higher than the edge minima.

The DFT-D calculations predict a large range of relative angular orientations of the 1NpOH and S moieties in the different isomers. More than half of the isomers are predicted to be $C_1$ symmetric and thus exist as a pair of enantiomers. Furthermore, different DFT methods predict different isomer geometries, so the structures shown in the figures should be considered as examples. The calculated Cartesian coordinates of all the complexes using all three methods are given in Tables S1–S34 of the supplementary material.

The edge isomers exhibit four different intermolecular contact types, where each isomer exhibits two of the four contact types:

(1) Classical OH···X (X = O, S) hydrogen bonds from the naphthol OH group to a lone-pair of the X atom. These (O)H···X distances are short, with $R \sim 1.75 - 1.80$ Å.
(2) Nonclassical OH···π interactions, which involve a close contact between the OH group and an aromatic C atom, an aromatic C=C bond, or an aromatic heteroatom X. The (O)H···X distances are typically $R \sim 1.90 - 2.05$ Å.
(3) Nonclassical CH···X (X = O, S) contacts, with H···X distances of $R \sim 2.20 - 2.40$ Å.
(4) (C)H···C contacts with long distances $R \sim 2.85$ Å, corresponding to the sum of van der Waals (vdW) radii or longer.

Figure 6 shows the ωB97X-D calculated isomers 1 and 2 of the 1NpOH·thiophene complex. Isomer 1 exhibits an OH···S hydrogen bond and a CH···C vdW contact. Isomer 2 combines a nonclassical OH···π hydrogen bond and CH···π vdW contact. Figure 7 shows the B97-D3 calculated isomers 1 and 2 of the 1NpOH·furan complex. Isomer 1 is similar to isomer 1 of the thiophene complex in combining an OH···O with a CH···π vdW contact. Isomer 2 combines OH···π and CH···O hydrogen bonds.

Figure 8 shows the edge isomer 1 of the 1NpOH·2,5-DMF complex, which is $C_s$ symmetric. Its OH···O(furan) hydrogen-bond distance is 1.92 Å. The edge isomer 2 is

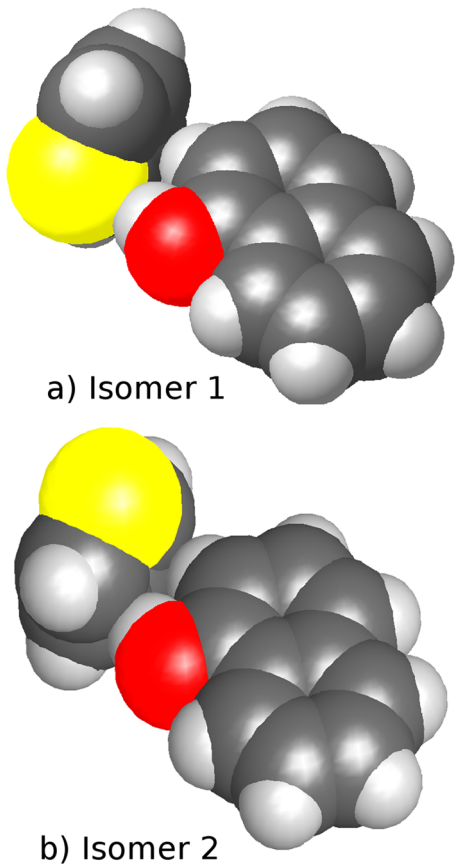


FIG. 6. ωB97X-D calculated structures of the 1-naphthol·thiophene edge complexes: (a) Isomer 1 and (b) isomer 2. For additional views of the two isomers, see Fig. S6 of the supplementary material. Cartesian coordinates are given in Tables S8 and S11 of the supplementary material.

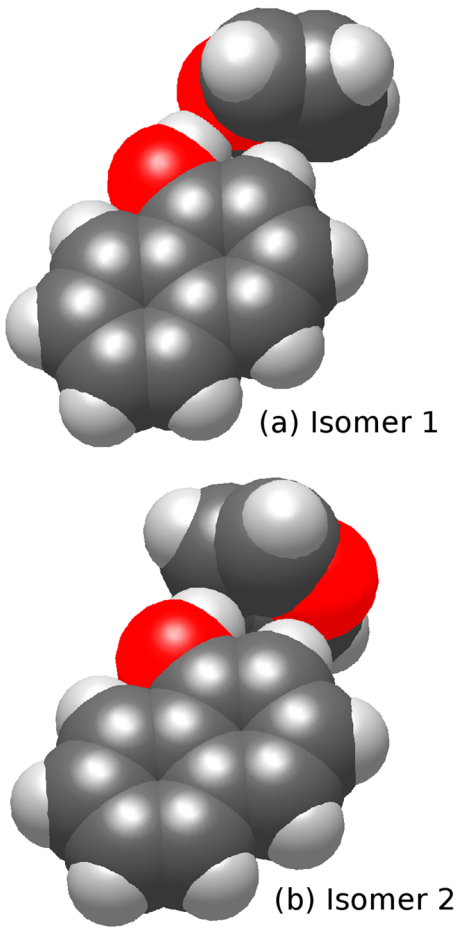


FIG. 7. B97-D3 calculated structures of the 1-naphthol·furan edge complexes: (a) isomer 1 ($C_s$ symmetric) and (b) isomer 2 (no symmetry). For Cartesian coordinates, see Tables S17 and S19 of the supplementary material.

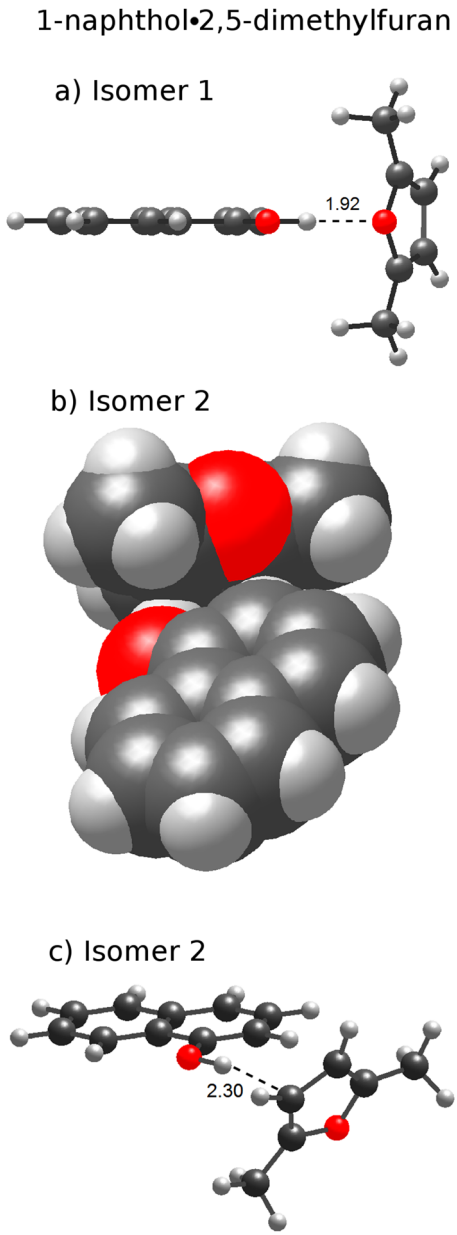


FIG. 8. B97-D3 calculated structures of the 1-naphthol·2,5-dimethylfuran edge complexes: (a) Isomer 1 ($C_s$ symmetric). (b) Isomer 2, space-filling representation; note that the 2,5-dimethylfuran moiety is strongly rotated relative to isomer 1. (c) Isomer 2, in ball-and-stick representation. For Cartesian coordinates of isomers 1 and 2, see Tables S27 and S30 of the supplementary material.

predicted to be 1-4 kJ/mol less stable than isomer 1. The space-filling model in Fig. 8(b) shows the proximity of one methyl group to the naphthalene plane. The ball-and-stick representation in Fig. 8(c) shows the OH$\cdots\pi$ hydrogen bond, which is predicted to be 0.38 Å longer than the OH$\cdots$O H-bond distance of isomer 1.

Figure 9 shows the B97-D3 calculated structure of isomer 3 of the 1NpOH·THF complex. The calculated $D_0(S_0)$ values of the other isomers are 0.15-1.5 kJ/mol smaller. For this complex, all the calculated isomers exhibit short and well-aligned OH$\cdots$O hydrogen bonds with the THF unit twisted away from the plane of the 1NpOH moiety. The THF subunit of isomer 2 exists in two pseudorotational forms (see Sec. III A).

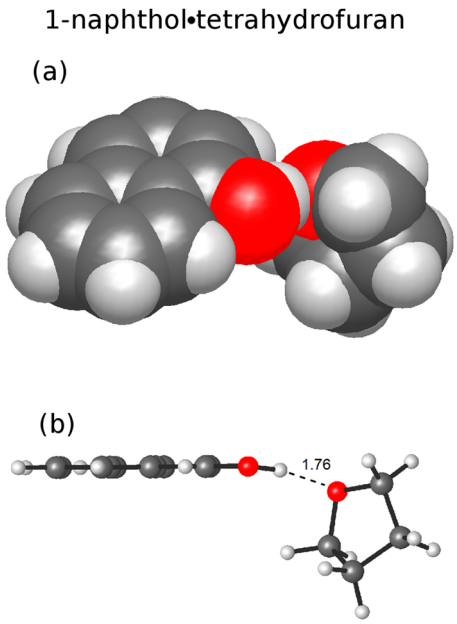


FIG. 9. B97-D3 calculated structure of the most stable 1-naphthol·tetrahydrofuran edge isomer 3: (a) space-filling representation, showing the OH$\cdots$O contact. (b) Ball-and-stick representation. For Cartesian coordinates, see Table S32 of the supplementary material.

## IV. DISCUSSION

### A. Complex structures and spectral shifts

Figure 1 shows that the complexes investigated in this work exhibit spectral shifts between $\delta\tilde{\nu} = -69$ cm$^{-1}$ for 1NpOH·thiophene and $\delta\tilde{\nu} = -184$ cm$^{-1}$ for 1NpOH·THF. As discussed above, large spectral red shifts are typical for edge complexes involving classical or nonclassical hydrogen bonds. The UV/UV-holeburning spectra did not reveal any isomers with small spectral shifts. We therefore assign all the complexes as edge complexes. If face isomers are transiently formed during the supersonic jet expansion, they rapidly isomerize to the more stable edge counterparts.

The spectral shift of the thiophene complex ($\delta\tilde{\nu} = -69$ cm$^{-1}$) is close to those of 1NpOH·benzene ($\delta\tilde{\nu} = -66$ cm$^{-1}$)[23] and to that of the edge isomer of 1NpOH·cyclopropane ($\delta\tilde{\nu} = -72$ cm$^{-1}$).[49] The structure of 1NpOH·benzene has been determined by rotational coherence spectroscopy (RCS); the benzene ring is orthogonal to the naphthalene ring and is arranged symmetrically with respect to the naphthalene plane.[55] The geometry of the cyclopropane complex has not yet been experimentally determined, but DFT-D (PBE0-D3) and high-level correlated calculations predict an edge structure with the 1NpOH OH group pointing to the center of a cyclopropane CC bond.[49]

These similarities motivated a closer comparison. We performed calculations for the benzene and cyclopropane complexes using the same DFT-D methods as above. The B97-D3 calculated structure of 1NpOH·benzene is shown in Fig. 10. The $\sigma_h$ symmetry plane of benzene is orthogonal to that of the 1NpOH moiety and the NpOH forms OH$\cdots\pi$ and CH$\cdots\pi$ hydrogen bonds with the benzene ring. This geometry is in good agreement with the RCS structure proposed by Felker.[55] The B97-D3 calculated structure of 1NpOH·cyclopropane is

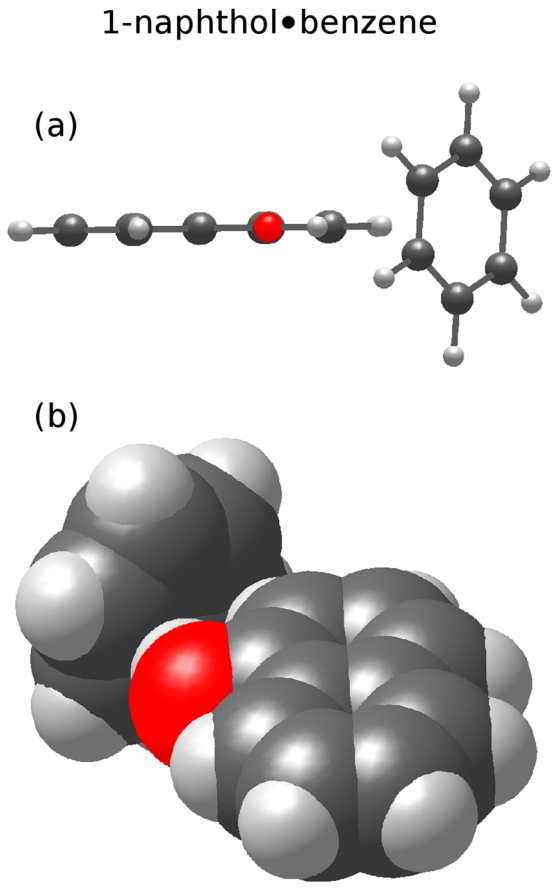


FIG. 10. B97-D3 calculated structure of the 1-naphthol·benzene edge isomer. (a) Ball-and-stick and (b) space-filling representations, showing the OH$\cdots\pi$ and CH$\cdots\pi$ contacts. For Cartesian coordinates, see Table S35 of the supplementary material.

shown in Fig. 11. It exhibits a single nonclassical H-bond from the naphthol OH group to the center of a cyclopropane C-C bond. The $\sigma_h$ plane of cyclopropane is perpendicular to that

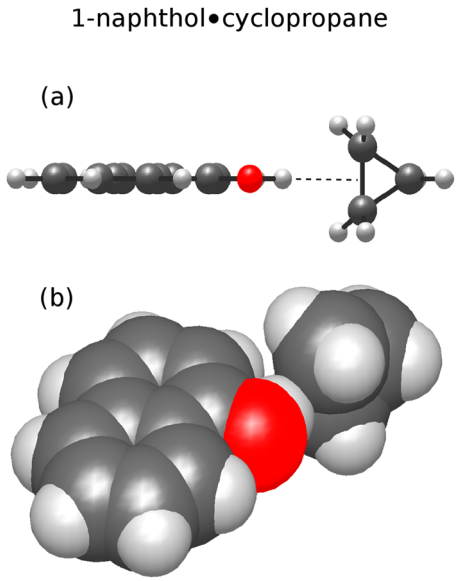


FIG. 11. B97-D3 calculated structure of the 1-naphthol·cyclopropane edge isomer. (a) Ball-and-stick and (b) space-filling representations, showing the OH contact to one of the cyclopropane C—C bonds. For Cartesian coordinates, see Table S36 of the supplementary material.

of the 1NpOH ring, but is oriented away from the 1NpOH, roughly along the OH bond axis. The B97-D3, B3LYP-D3, and $\omega$B97X-D structures of the cyclopropane complex are very similar to those previously calculated with PBE0-D3 and high-level correlated methods.[49]

The structures of the high-symmetry complexes involving benzene and cyclopropane moieties lend themselves to interpretation in terms of nonclassical hydrogen bonds. However, the different isomers of the thiophene, furan, 2,5-DMF, and THF edge complexes cover a large range of geometries. Some of these isomers are difficult to describe in terms of H-bond interactions, either because the putative H-bond with the admolecule originates from the weak CH donor and is long (i.e., a van der Waals contact distance or longer) or because the heteroatom (O, S) does not lie in the 1NpOH plane and the admolecule is tilted relative to the 1NpOH plane.

### B. Experimental dissociation energies

In the first data column of Table III, we collect the experimental dissociation energies of the 1-naphthol·S complexes and compare them to the calculated B97-D3, B3LYP-D3, and $\omega$B97X-D $D_0$ values. The experimental and calculated $D_0$ values are also compared in Fig. 12, where both are plotted vs. the isotropic (average) electronic polarizability $\bar{\alpha}$ of the S admolecule. Since each computational method predicts several isomers with different dissociation energies and we have no way of determining the structures in our experiment, we compare the experimental $D_0$ to that of the isomer with the *largest* dissociation energy predicted by the given DFT-D method.

The $D_0$ = 15.34 kJ/mol of the cyclopropane complex is about half of those of the classically H-bonded complexes shown in the upper part of Fig. 12 such as 1NpOH·oxirane and 1NpOH·oxetane. This much smaller $D_0$ is characteristic for nonclassical hydrogen bonding.

Replacing the nonaromatic cyclopropane by the aromatic furan increases the $D_0$ of the 1NpOH complex by 42%. The average electronic polarizability of furan ($\bar{\alpha}$ = 7.4 Å$^3$) is 30% larger than that of cyclopropane ($\bar{\alpha}$ = 5.66 Å$^3$), so the increase in $D_0$ for the furan complex is larger than would be expected from the relative polarizabilities; see Fig. 12. However, the $D_0$ of the complex with the polarizable benzene molecule ($\bar{\alpha}$ = 8.89 Å$^3$) is slightly *smaller* than that of the furan complex; see also Table III and Fig. 12. Since cyclopropane and benzene are nonpolar, there is no dipole-dipole-interaction with the dipole moment of 1NpOH, in contrast to furan. We propose that the larger $D_0$ of the 1NpOH·furan complex is due to this additional electrostatic interaction.

The average polarizability of thiophene ($\bar{\alpha}$ = 9.8 Å$^3$) is only 10% larger than that of benzene, but the thiophene complex has a 25% larger $D_0$. Again, the $D_0$ increase is larger than expected from the relative polarizabilities of the two admolecules, suggesting that electrostatic and inductive contributions contribute to the larger stability of the thiophene complex. By contrast, the $D_0$ increase from furan to thiophene is roughly proportional to $\bar{\alpha}$.

A large $D_0$ increase by ~75% occurs upon going from the unsaturated furan to the saturated tetrahydrofuran. As

TABLE III. Experimental and calculated $S_0$ state dissociation energies $D_0(S_0)$ (in kJ/mol) of the H-bonded 1-naphthol complexes with cyclopropane, benzene, furan, thiophene, 2,5-dimethylfuran, and tetrahydrofuran. The calculated vibrational zero-point energy changes ΔVZPE are given in parentheses. Calculations employed the dispersion-corrected DFT methods B97-D3, B3LYP-D3, and ωB97X-D. For each complex, the calculated $D_0$ in best agreement with experiment is marked in bold.

| Complex | Experimental | B97-D3 $D_0$ (ΔVZPE) | B3LYP-D3 $D_0$ (ΔVZPE) | ωB97X-D $D_0$ (ΔVZPE) |
|---|---|---|---|---|
| Furan | 21.82 ± 0.29 | 21.58 (2.74)[a] | **21.81** (2.97)[a] | 19.89 (3.18)[a] |
| Thiophene | 26.56 ± 0.57 | **24.15** (2.81)[a] | 23.76 (2.80)[a] | 20.77 (3.19)[a] |
| 2,5-Dimethylfuran | 36.5 ± 2.3 | 29.69 (4.32)[b] | **32.41** (4.33)[b] | 29.83 (5.03)[b] |
| Tetrahydrofuran | 37.63 ± 1.29 | 36.61 (5.55)[a] | 38.94 (5.86)[a] | **37.34** (6.00)[b] |
| Cyclopropane edge[c] | 15.34 ± 0.03 | 15.79 (3.63) | **15.51** (3.68) | 14.61 (4.27) |
| Benzene[d] | 21.21 ± 0.30 | 23.28 (2.64) | 23.13 (2.59) | **21.53** (2.94) |
| Mean absolute deviation (MAD) | | 2.2 | 1.7 | 2.6 |

[a]Calculated values for the most stable isomer 2.
[b]Calculated values for the most stable isomer 1.
[c]From Ref. 49.
[d]From Ref. 23.

can be seen in Fig. 12, the electronic polarizability of THF ($\bar{\alpha}$ = 7.97 Å$^3$) is only 8% larger than that of furan. This pair of complexes clearly exemplifies the difference between nonclassical H-bonding (with mainly dispersion contributions) and classical H-bonding (mainly electrostatic and inductive contributions). Accordingly, the 1NpOH·THF complex exhibits a short H-bond with one of the ether oxygen lone-pairs; see Fig. 9.

Interestingly, a similar $D_0$ increase by ~75% occurs when adding two methyl groups to furan. Figure 12 shows that the polarizability of 2,5-DMF ($\bar{\alpha}$ = 11.09 Å$^3$) is 40% larger than that of furan. Here, we attribute the $D_0$ increase of the 2,5-DMF complex mainly to the increase of dispersion interactions with the 1NpOH moiety; a more detailed discussion is given in Sec. IV D.

### C. Calculated and experimental dissociation energies

The experimental and calculated dissociation energies are compared in Table III. The DFT-D calculated $D_0$ values for 1NpOH·cyclopropane agree nicely with experiment, the B3LYP-D3 value being within 0.17 kJ/mol, the B97-D3 value only slightly larger, and the ωB97X-D value being slightly lower. For the 1NpOH·benzene complex, the calculated B97-D3 and B3LYP-D3 $D_0$ values are about 2 kJ/mol larger than experiment, while the ωB97X-D value is only 0.3 kJ/mol larger. For the 1NpOH·furan complex, the B3LYP-D3 and B97-D3 $D_0$ values lie within the experimental $D_0$ brackets, while the ωB97X-D value is about 2 kJ/mol too low.

In contrast to these good agreements, the experimental $D_0$ of the 1NpOH·thiophene complex is ~2.7 kJ/mol

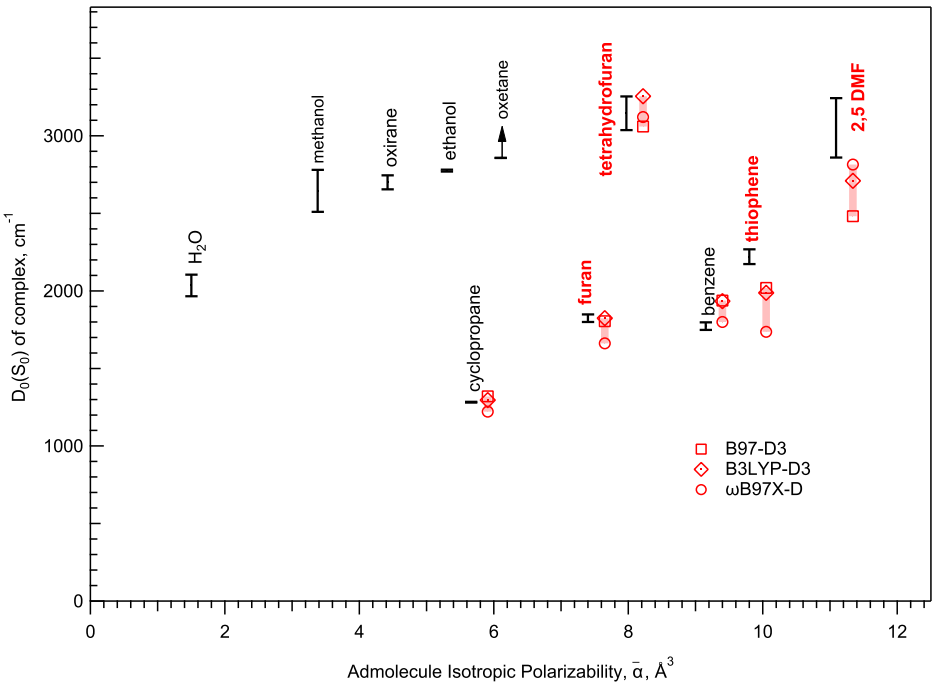


FIG. 12. Experimental ground-state dissociation energies $D_0(S_0)$ of the hydrogen bonded 1-naphthol·S complexes measured in this and previous work (Refs. 23, 27, 48, and 49) plotted vs. the isotropic electronic polarizability $\bar{\alpha}$ of the admolecule S (in Å$^3$). Values from this work are labeled in red, and previous values in black. The $D_0$ values are calculated in this work with the B97-D3, B3LYP-D3, and ωB97X-D methods; they are offset to the right and are indicated in red.

larger than the B97-D3 and B3LYP-D3 calculated values and nearly 6 kJ/mol larger than the $\omega$B97X-D $D_0$. Notably, none of the calculated $D_0$ values lies within the brackets of the experimental measurement; see Fig. 12. The lack of agreement may stem from different errors of the DFT calculations (insufficiently large basis set, problems with the short-range exchange-correlation, with D3 in general, missing many-body dispersion).

For the THF complex, all three calculated $D_0(S_0)$ values lie within the experimental $D_0$ brackets although these are wider than for the other complexes and do not constitute such a stringent test for the DFT-D methods as discussed above for the cyclopropane, furan, and benzene complexes. Although the experimental $D_0$ brackets are even wider for the 2,5-DMF complex, the agreement between calculations and experiment is much poorer than for the THF complex, with all three values being below the lower $D_0$ bracket.

### D. Correlation of nonclassical H-bonding energies with D3 dispersion interactions

As noted above for the nonclassically H-bonded complexes cyclopropane, furan, benzene, and thiophene, the experimental $D_0$ values correlate well with the isotropic electronic polarizability $\bar{\alpha}$ of the admolecule. However, given that the polarizabilities $\alpha$(S) and $\alpha$(1NpOH) are tensors and that the dispersion interaction depends on the relative orientation of the 1NpOH and S moieties, the dispersion stabilization is only roughly modeled by $\bar{\alpha}$. An alternative is to calculate the dispersion interaction energy in terms of atom-atom-interactions at the minimum-energy geometry of the complex using the D3 method. For this, we employed the DFT-D3 parameters[60] and the D3 program code on the Grimme web page[67] (note that the latter may or may not be identical to the implementation of the D3 calculation in Gaussian 16).

In Fig. 13, we plot the experimental dissociation energies $D_0(S_0)$ vs. the calculated D3-energies at the respective minimum-energy geometries. The $D_0$'s of the nonclassically H-bonded cyclopropane, furan, benzene, and thiophene complexes correlate nicely with the calculated D3 part of the binding energy. The fact that the experimental $D_0$ for the THF complex lies ~1100 cm$^{-1}$ above the dashed $D_0$ = D3 line suggests that there the non-dispersion (electrostatic, inductive, and charge-transfer) stabilizing contributions to the interaction energy are important. As expected from its larger polarizability, the 2,5-DMF complex also exhibits a larger D3-contribution to its binding energy than cyclopropane, furan, benzene, and thiophene. However, the experimental $D_0$ lies ~600 cm$^{-1}$ above the dashed line, implying that the non-dispersion (electrostatic, inductive, etc.) stabilizing contributions also increase in this complex, relative to the furan complex.

Without the D3 dispersion corrections, the cyclopropane and benzene complexes are predicted *not* to be bound at their equilibrium geometries (calculated with the D3 correction) and the furan and thiophene complexes are calculated to be only weakly bound. By contrast, the THF and 2,5-DMF complexes are predicted to be bound even without the D3 correction.

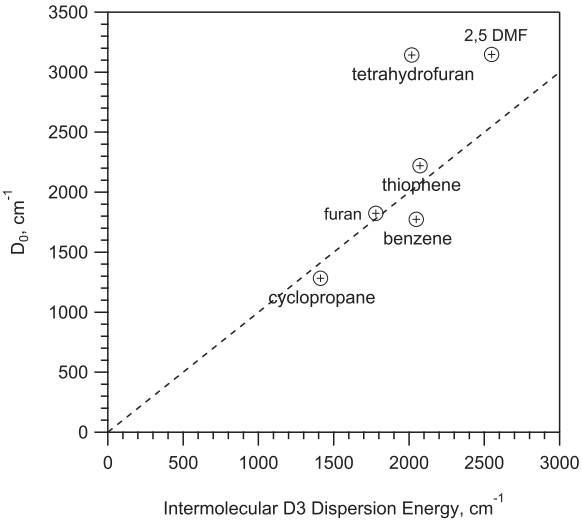


FIG. 13. Experimental dissociation energies $D_0(S_0)$ of the six hydrogen-bonded 1NpOH·S complexes discussed above, plotted vs. the calculated D3-dispersion contributions to the intermolecular binding energy.[60,67] The dashed line marks $D_0(S_0)$ = D3, showing the good correlation of $D_0(S_0)$ with the D3 contribution for the cyclopropane, furan, benzene, and thiophene complexes; see the text.

This again implies that the non-dispersion contributions to the H-bonding are large for the latter two complexes.

## V. CONCLUSIONS

We have determined the $S_0$ and $S_1$ state intermolecular dissociation energies $D_0$ of the 1-naphthol·S hydrogen-bonded complexes with S = furan, 2,5-dimethylfuran, thiophene, and tetrahydrofuran using the stimulated-emission pumping resonant two-photon ionization (SEP-R2PI) method. The $D_0$ of the furan complex was bracketed within 0.3 kJ/mol, corresponding to a relative uncertainty of ±1.3%. The dissociation energies increase by 1-2 kJ/mol upon $S_0 \rightarrow S_1$ excitation of the 1-naphthol moiety.

In parallel, the structures, binding energies $D_e$, vibrational frequencies, changes of vibrational zero-point energy ($\Delta$VZPE), and dissociation energies $D_0$ were calculated using the dispersion-corrected density functional methods B97-D3, B3LYP-D3, and $\omega$B97X-D. All methods predict that hydrogen-bonded edge structures in which the 1-naphthol OH group acts as an H-bond donor are most stable. While all methods also predict face isomers that are bound by dispersion interactions, their calculated $D_0$ values are smaller than those of the edge isomers. This agrees with the lack of experimental observation of any face isomers.

The dissociation energies calculated with the three methods differ mutually by 6%-15%. Relative to experiment, the B3LYP-D3 method reproduced the experimental $D_0$ values best, with a minimum deviation of −0.01 kJ/mol (for the furan complex), a mean absolute deviation (MAD) of 1.7 kJ/mol, and a maximum difference of 4.1 kJ/mol (for the 2,5-dimethylfuran complex). The B97-D3 method exhibits a larger MAD of 2.2 kJ/mol and a larger maximum difference of 6.8 kJ/mol, again for 1-naphthol·2,5-dimethylfuran. The $\omega$B97X-D method generally predicts the smallest dissociation energies of the three methods and exhibits the largest differences relative to

experiment, with a MAD of 2.6 kJ/mol and a maximum difference of 6.67 kJ/mol for 1-naphthol·2,5-dimethylfuran. Overall the predictive performances of the three DFT-D methods are encouraging, but the computational MADs are significantly larger than the mean absolute experimental bracketing width, which is ±0.8 kJ/mol, averaged over the same six complexes.

We compared the $D_0(S_0)$ values measured here with those of the nonclassically H-bonded complexes 1NpOH·cyclopropane and 1NpOH·benzene and of the classically H-bonded complexes of 1NpOH with $H_2O$, alcohols, and cyclic ethers.[23,27,49,53] Plotting $D_0(S_0)$ vs. the average molecular polarizability $\bar{\alpha}$(S) reveals very different dependencies for nonclassically and classically H-bonded complexes: The $D_0$ values of the non-classically H-bonded complexes increase roughly linearly with increasing $\bar{\alpha}$(S) of the solvent, suggesting that the dispersion part of the interaction energy is the dominating contribution to non-classical H-bonds. This is supported by the calculated D3 contributions to the intermolecular binding energy, which also show a near-linear correlation of $D_0$ with the D3 energy. By contrast, the classically H-bonded complexes exhibit a steep initial rise of $D_0$ with $\bar{\alpha}$(S), reaching larger $D_0$ values than for the nonclassically H-bonded complexes, which is then followed by a slower increase with $\bar{\alpha}$(S). This implies that the dispersion part of the interaction energy contributes less to the total energy in classically H-bonded complexes. Since both $D_0$ and $\bar{\alpha}$(S) are experimental quantities, this $D_0$ vs. $\bar{\alpha}$(S) pattern allows us to *experimentally* differentiate nonclassically and classically H-bonded complexes.

We suggest that intermolecular energy partitioning methods such as SAPT (symmetry-adapted perturbation theory)[68] or DFT-SAPT[69–71] be applied to these edge complexes in order to deepen the understanding of the different energy contributions to their binding energies and possibly assist in the development of improved theoretical methods.

## SUPPLEMENTARY MATERIAL

See supplementary material for a SEP-R2PI scheme (Fig. S1), UV/UV hole-burning and probe laser spectra (Figs. S2–S5), views of calculated structures (Figs. S6 and S7), and Cartesian coordinates of the 1-naphthol·S complexes optimized by the three DFT-D methods (Tables S1 to S36).

## ACKNOWLEDGMENTS

We thank the Swiss National Science Foundation for financial support (Grant No. 200021E-160404). A. Poblotzki (Universität Göttingen) was additionally funded by a travel grant of the Priority Program No. SPP1807 "*Control of London dispersion interactions in molecular chemistry*" of the Deutsche Forschungsgemeinschaft (Project No. 271107160).

[1]G. A. Jeffrey, *An Introduction to Hydrogen Bonding* (Oxford University Press, Oxford, 1997).
[2]J. E. Del Bene and M. J. T. Jordan, Int. Rev. Phys. Chem. **18**, 119 (1999).
[3]G. A. Jeffrey and W. Saenger, *Hydrogen Bonding in Biological Structures* (Springer, Berlin, 1991).
[4]G. R. Desiraju and T. Steiner, *The Weak Hydrogen Bond in Structural Chemistry and Biology* (Oxford University Press, 2001).
[5]T. Steiner, Angew. Chem., Int. Ed. **41**, 48 (2002).
[6]G. R. Desiraju, Acc. Chem. Res. **35**, 565 (2002).
[7]S. Grimme, J. Comput. Chem. **25**, 1463 (2004).
[8]S. Grimme, J. Comput. Chem. **27**, 1787 (2006).
[9]J.-D. Chai and M. Head-Gordon, Phys. Chem. Chem. Phys. **10**, 6615 (2008).
[10]L. Goerigk and S. Grimme, J. Chem. Theory Comput. **7**, 291 (2011).
[11]L. Goerigk and S. Grimme, Phys. Chem. Chem. Phys. **13**, 6670 (2011).
[12]W. Hujo and S. Grimme, Phys. Chem. Chem. Phys. **13**, 13942 (2011).
[13]P. Jurečka, J. Šponer, J. Černy, and P. Hobza, Phys. Chem. Chem. Phys. **8**, 1985 (2006).
[14]J. Řezáč, K. E. Riley, and P. Hobza, J. Chem. Theory Comput. **7**, 2427 (2011).
[15]J. Řezáč, K. E. Riley, and P. Hobza, J. Chem. Theory Comput. **7**, 3466 (2011).
[16]J. Řezáč and P. Hobza, J. Chem. Theory Comput. **8**, 141 (2012).
[17]R. Podeszwa, K. Patkowski, and K. Szalewicz, Phys. Chem. Chem. Phys. **12**, 5974 (2010).
[18]T. Takatani, E. G. Hohenstein, M. Malagoli, M. S. Marshall, and C. D. Sherrill, J. Chem. Phys. **132**, 144104 (2010).
[19]D. E. Taylor, J. G. Angyan, G. Galli, C. Zhang, F. Gygi, K. Hirao, J. W. Song, K. Rahul, O. A. von Lilienfeld, R. Podeszwa, I. W. Bulik, T. M. Henderson, G. E. Scuseria, J. Toulouse, R. Peverati, D. G. Truhlar, and K. Szalewicz, J. Chem. Phys. **145**, 124105 (2016).
[20]J. F. Ogilvie and F. Y. H. Wang, J. Mol. Struct. **273**, 277 (1992).
[21]J. F. Ogilvie and F. Y. H. Wang, J. Mol. Struct. **291**, 313 (1993).
[22]R. A. Mata and M. A. Suhm, Angew. Chem., Int. Ed. **56**, 11011 (2017).
[23]C. Wickleder, T. Droz, T. Bürgi, and S. Leutwyler, Chem. Phys. Lett. **264**, 257 (1997).
[24]J. E. Braun, T. L. Grebner, and H. J. Neusser, J. Phys. Chem. A **102**, 3273 (1998).
[25]J. E. Braun, T. Mehnert, and H. J. Neusser, Int. J. Mass Spectrom. **203**, 1 (2000).
[26]M. Mons, I. Dimicoli, and F. Piuzzi, Int. Rev. Phys. Chem. **21**, 101 (2002).
[27]C. Wickleder, D. Henseler, and S. Leutwyler, J. Chem. Phys. **116**, 1850 (2002).
[28]J. A. Frey, C. Holzer, W. Klopper, and S. Leutwyler, Chem. Rev. **116**, 5614 (2016).
[29]S. Georgiev and H. Neusser, J. Electron Spectrosc. Relat. Phenom. **142**, 207 (2005).
[30]J. L. Knee, L. R. Khundkar, and A. H. Zewail, J. Chem. Phys. **87**, 115 (1987).
[31]H. Abe, N. Mikami, and M. Ito, J. Phys. Chem. **86**, 1768 (1982).
[32]A. J. Gotch and T. S. Zwier, J. Chem. Phys. **96**, 3388 (1992).
[33]A. Courty, M. Mons, I. Dimicoli, F. Piuzzi, M.-P. Gaigeot, V. Brenner, P. de Pujo, and P. Millié, J. Phys. Chem. A **102**, 6590 (1998).
[34]B. E. Rocher-Casterline, L. C. Ch'ng, A. K. Mollner, and H. Reisler, J. Chem. Phys. **134**, 211101 (2011).
[35]L. C. Ch'ng, A. K. Samanta, G. Czakó, J. M. Bowman, and H. Reisler, J. Am. Chem. Soc. **134**, 15430 (2012).
[36]A. K. Samanta, L. C. Ch'ng, and H. Reisler, Chem. Phys. Lett. **575**, 1 (2013).
[37]L. C. Chng, A. K. Samanta, Y. Wang, J. M. Bowman, and H. Reisler, J. Phys. Chem. A **117**, 7207 (2013).
[38]A. K. Samanta, Y. Wang, J. S. Mancini, J. M. Bowman, and H. Reisler, Chem. Rev. **116**, 4913 (2016).
[39]K. E. Riley, M. Pitoňák, P. Jurečka, and P. Hobza, Chem. Rev. **110**, 5023 (2010).
[40]S. Grimme, A. Hansen, J. G. Brandenburg, and C. Bannwarth, Chem. Rev. **116**, 5105 (2016).
[41]C. Holzer and W. Klopper, Mol. Phys. **115**, 2775 (2017).
[42]C. Holzer and W. Klopper, J. Chem. Phys. **147**, 181101 (2017).
[43]T. Bürgi, T. Droz, and S. Leutwyler, Chem. Phys. Lett. **225**, 351 (1994).
[44]T. Droz, T. Bürgi, and S. Leutwyler, J. Chem. Phys. **103**, 4035 (1995).
[45]T. Droz, T. Bürgi, and S. Leutwyler, Ber. Bunsenges. Phys. Chem. **99**, 429 (1995).
[46]S. Leutwyler and J. Jortner, J. Phys. Chem. **91**, 5558 (1987).
[47]N. Ben-Horin, U. Even, J. Jortner, and S. Leutwyler, J. Chem. Phys. **97**, 5296 (1992).
[48]T. Bürgi, T. Droz, and S. Leutwyler, J. Chem. Phys. **103**, 7228 (1995).
[49]S. Maity, R. Knochenmuss, C. Holzer, G. Féraud, J. A. Frey, W. Klopper, and S. Leutwyler, J. Chem. Phys. **145**, 164304 (2016).
[50]S. Maity, P. Ottiger, F. A. Balmer, R. Knochenmuss, and S. Leutwyler, J. Chem. Phys. **145**, 244314 (2016).

[51]R. Knochenmuss, S. Maity, and S. Leutwyler, Chimia **71**, 7 (2017).
[52]R. Knochenmuss, R. K. Sinha, and S. Leutwyler, J. Chem. Phys. **148**, 134302 (2018).
[53]T. Bürgi, T. Droz, and S. Leutwyler, Chem. Phys. Lett. **246**, 291 (1995).
[54]R. Knochenmuss, S. Maity, F. Balmer, C. Müller, and S. Leutwyler, J. Chem. Phys. **149**, 034306 (2018).
[55]P. M. Felker and A. H. Zewail, in *Femtosecond Chemistry*, edited by J. Manz and L. Wöste (VCH, Weinheim, 1995), Vol. I, Chap. 5.
[56]A. Poblotzki, J. Altnöder, and M. A. Suhm, Phys. Chem. Chem. Phys. **18**, 27265 (2016).
[57]A. Poblotzki, H. C. Gottschalk, and M. Suhm, J. Phys. Chem. Lett. **8**, 5656 (2017).
[58]H. C. Gottschalk, A. Poblotzki, M. A. Suhm, M. M. Al-Mogren, J. Antony, A. A. Auer, L. Baptista, D. M. Benoit, G. Bistoni, F. Bohle, R. Dahmani, D. Firaha, S. Grimme, A. Hansen, M. E. Harding, M. Hochlaf, C. Holzer, G. Jansen, W. Klopper, W. A. Kopp, L. C. Kröger, K. Leonhard, H. Mouhib, F. Neese, M. N. Pereira, I. S. Ulusoy, A. Wuttke, and R. A. Mata, J. Chem. Phys. **148**, 014301 (2018).
[59]L. Goerigk and S. Grimme, J. Chem. Phys. **132**, 184103 (2010).
[60]S. Grimme, J. Antony, S. Ehrlich, and H. Krieg, J. Chem. Phys. **132**, 154104 (2010).
[61]M. J. Frisch, G. W. Trucks, H. B. Schlegel, G. E. Scuseria, M. A. Robb, J. R. Cheeseman, G. Scalmani, V. Barone, G. A. Petersson, H. Nakatsuji, X. Li, M. Caricato, A. V. Marenich, J. Bloino, B. G. Janesko, R. Gomperts, B. Mennucci, H. P. Hratchian, J. V. Ortiz, A. F. Izmaylov, J. L. Sonnenberg, D. Williams-Young, F. Ding, F. Lipparini, F. Egidi, J. Goings, B. Peng, A. Petrone, T. Henderson, D. Ranasinghe, V. G. Zakrzewski, J. Gao, N. Rega, G. Zheng, W. Liang, M. Hada, M. Ehara, K. Toyota, R. Fukuda, J. Hasegawa, M. Ishida, T. Nakajima, Y. Honda, O. Kitao, H. Nakai, T. Vreven, K. Throssell, J. A. Montgomery, Jr., J. E. Peralta, F. Ogliaro, M. J. Bearpark, J. J. Heyd, E. N. Brothers, K. N. Kudin, V. N. Staroverov, T. A. Keith, R. Kobayashi, J. Normand, K. Raghavachari, A. P. Rendell, J. C. Burant, S. S. Iyengar, J. Tomasi, M. Cossi, J. M. Millam, M. Klene, C. Adamo, R. Cammi, J. W. Ochterski, R. L. Martin, K. Morokuma, O. Farkas, J. B. Foresman, and D. J. Fox, GAUSSIAN 16, Revision A.03, Gaussian, Inc., Wallingford, CT, 2016.
[62]F. A. Balmer, P. Ottiger, C. Pfaffen, and S. Leutwyler, J. Phys. Chem. A **117**, 10702 (2013).
[63]F. A. Balmer, P. Ottiger, and S. Leutwyler, J. Phys. Chem. A **119**, 10462 (2015).
[64]A. Amirav and J. Jortner, Chem. Phys. **85**, 19 (1984).
[65]J. Bösiger and S. Leutwyler, Chem. Rev. **90**, 489 (1990).
[66]V. A. Rayón and J. L. Sordo, J. Chem. Phys. **122**, 204303 (2005).
[67]See https://www.chemie.uni-bonn.de/pctc/mulliken-center/software/dft-d3/ for more information on the DFT-D3 dispersion correction.
[68]B. Jeziorski, K. Szalewicz, and G. Chalasinski, Int. J. Quantum Chem. **14**, 271 (1978).
[69]A. Hesselmann, G. Jansen, and M. Schütz, J. Chem. Phys. **122**, 014103 (2005).
[70]T. M. Parker, L. A. Burns, R. M. Parrish, A. G. Ryno, and C. D. Sherrill, J. Chem. Phys. **140**, 094106 (2014).
[71]G. Jansen, Wiley Interdiscip. Rev.: Comput. Mol. Sci. **4**, 127 (2014).